Aust. J. Phys., 1983, **36**, 617–31

The Strangeness-exchange Reaction $K^-d \to \Lambda p\pi^-$ in Flight*

R. H. Dalitz[A] *and A. Deloff*[B]

[A] Department of Theoretical Physics, Oxford University, Oxford OX1 3NP, England.
[B] Institute for Nuclear Science and Technology, Hoza 69, Warsaw 00-681, Poland.

Abstract

The data on the forward reaction $K^-d \to \Lambda p\pi^-$ at 700 MeV/c are compared with calculations using semi-phenomenological one-boson-exchange hyperon–nucleon potentials and $\bar{K}N \to \pi Y$ amplitudes deduced from two-body data. This gives a new test of these potentials, since only the spin-triplet potentials are involved, in contrast with all other scattering data, which depend on a spin-weighted average of singlet and triplet contributions. However, this comparison does not yet provide an empirical distinction between Potential 1 of Brown *et al.* (1970) and Potential F of Nagels *et al.* (1979). The $\bar{K}N \to \pi\Sigma$ and $\bar{K}N \to \pi\Lambda$ amplitudes interfere in this reaction, so that its analysis can yield new knowledge of them; the present work requires a phase for the $\bar{K}N \to \pi\Lambda$ amplitude different by about $-135°$ from that deduced from partial-wave analyses.

1. Introduction

Little new data have become available on low-energy hyperon–nucleon cross sections in the past decade and it has therefore been natural to turn to consider the strangeness-exchange reactions

$$K^- + d \to Y + N + \pi, \tag{1}$$

Y being the generic symbol for (Λ, Σ) hyperons and N that for nucleons, since their characteristics must also reflect properties of the YN interactions, effective in the final state. Many groups have reported data on these reactions, both for K^- capture from rest and for the $K^- \to \pi^-$ strangeness-exchange reactions in flight. It is known (see e.g. Toker *et al.* 1981) that $\bar{K}N$ multiple-scattering effects are large in the initial K^-d system for K^- capture from rest or at low energies (say, for lab momentum $p_K < 200$ MeV/c). We therefore confine attention here to the simpler case of intermediate K^- momenta, of order 1000 MeV/c, where multiple-scattering effects (Glauber 1959) are believed to be of secondary importance, especially for a deuterium target.

The bulk of the data on deuterium has been obtained in bubble chamber experiments, and the reaction

$$K^-d \to \Lambda p\pi^- \tag{2}$$

* Dedicated to the memory of Professor S. T. Butler who died on 15 May 1982.

0004-9506/83/050617$02.00

has been particularly well studied by Cline *et al.* (1968) at 400 MeV/c, by Braun *et al.* (1977) over the range 680–840 MeV/c, by Sims *et al.* (1971) over the range 670–925 MeV/c, by Alexander *et al.* (1969) over the range 900–1100 MeV/c, and by Eastwood *et al.* (1971) at 1450 and 1650 MeV/c. These data all show a sharp peak at 2129 MeV in the Λp mass distribution, essentially coincident with the Σ^+n threshold mass $2128{\cdot}93 \pm 0{\cdot}06$ MeV (note that the Σ^0p threshold mass is $2130{\cdot}74 \pm 0{\cdot}08$ MeV). This striking phenomenon is clearly pertinent to the properties of the YN interaction in the nonrelativistic region (say, below $m_{YN} = 2200$ MeV). Indeed, because the peak stands out so well, these data are especially pertinent for the mass range 2129 ± 5 MeV, which is little known otherwise, there being no relevant data at all just below the Σ^+n threshold (or the charge-symmetric Σ^-p threshold) and rather little just above this threshold, owing to the short lifetimes for $\Sigma^\pm$ decay and the difficulty of measuring the short tracks appropriate to the study of ΣN interactions in hydrogen bubble chambers for momenta below about 100 MeV/c.

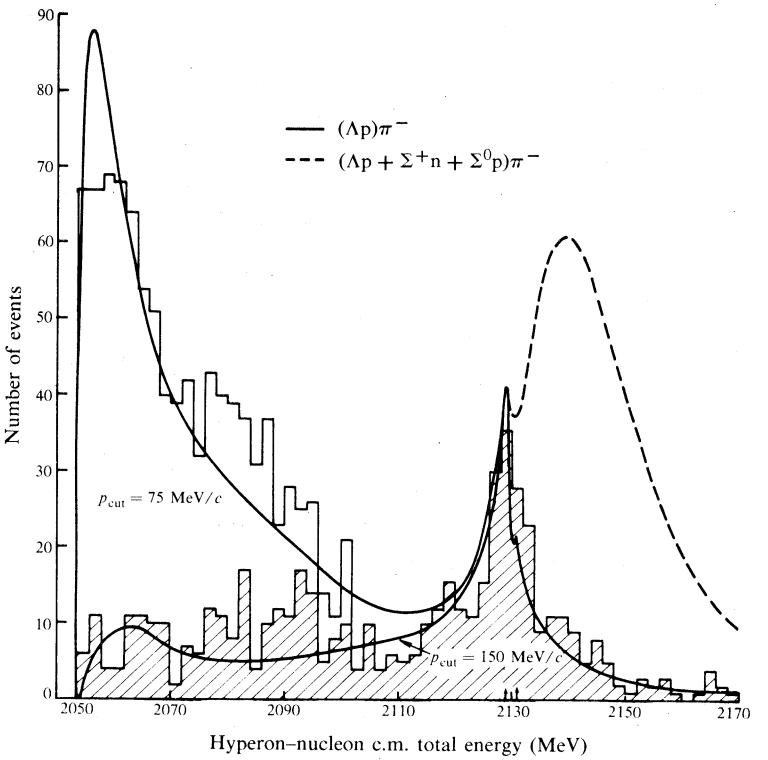

Fig. 1. Comparison of the calculated $m_{\Lambda p}$ distribution for the NRS-F YN potential (Nagels *et al.* 1979) and the 700 MeV/c Gopal amplitudes (with added phase $\phi = 135°$), for $\cos\theta_{K\pi} \geqslant 0{\cdot}9$, with the experimental data of Braun *et al.* (1977) (see text).

In the near future, we can look forward to new data on these reactions (1), from counter experiments giving good energy resolution and high statistics, and we expect that these will be very informative concerning the ΛN and ΣN systems in their threshold mass regions. One such experiment has already been reported (May *et al.*

1982), aimed specifically at the question of $I = \frac{3}{2}$ ΣN bound states*, and another is in preparation (E. V. Hungerford and H. Piekarz, personal communication 1982).

In the present paper, we shall focus attention on the experiment on reaction (2) by Braun *et al.* (1977) at 700 MeV/c, which is especially favourable in both statistics and energy resolution. The $m_{\Lambda p}$ mass distribution they have reported is reproduced here by the histogram in Fig. 1. Their data include only events where the final proton was measurable, having a track with projected length at least 1 mm. This corresponds roughly to a cut on the proton recoil momentum at $p_{\rm cut} = 75$ MeV/c. The effect on this distribution of increasing the cut to $p_{\rm cut} = 150$ MeV/c is shown by the shaded region in Fig. 1.

It has long been known (Feshbach and Kerman 1966; C. Rubbia, personal communication 1969; Bonazzola *et al.* 1970; Kerman and Lipkin 1971; Povh 1978) that there are special advantages in studying the reactions (1) near $\theta_{K\pi} = 0°$. Firstly, at $\theta_{K\pi} = 0°$, for total c.m. energy $m_{\rm YN}$ of the final YN system, there exists a 'magic momentum' for the incident K^- meson of

$$p_{K0} = \{\Pi(m_{\rm YN} - m_d \pm m_p \pm m_\pi)\}^{\frac{1}{2}}/2(m_{\rm YN} - m_d), \tag{3}$$

at which the momentum transfer q in the transition $d \to (YN)$ is zero. Above this magic momentum (3), q always increases with increasing p_K, but with an asymptotic value $(m_{\rm YN}^2 - m_d^2)/2m_{\rm YN}$. It also increases as p_K falls below p_{K0}, reaching the value

$$q_0 = \{\Pi(m_d + m_K \pm m_{\rm YN} \pm m_\pi)\}^{\frac{1}{2}}/2(m_K + m_d) \tag{4}$$

for $p_K = 0$, provided that $m_{\rm YN} + m_\pi \leqslant m_d + m_K$. In our case with $m_{\rm YN} \approx 2129$ MeV and $p_K = 700$ MeV/c, q has the value 93 MeV/c, so that the baryons are quite nonrelativistic. Since the wavelength $\hbar/q$ is then comparable with the deuteron radius, and the deuteron wavefunction is dominantly S state, the dominant transitions induced by $\boldsymbol{q}$ are S → S, just those necessary to reach the YN thresholds with nonzero amplitude. The second advantage is that the amplitude for the interaction $\overline{K}N \to \pi Y$, the primary interaction which transfers strangeness −1 to the two-baryon system, has no spin-flip component for $\theta_{K\pi} = 0°$. Since the deuteron is spin-triplet, being a superposition of ^3S and ^3D configurations, the final YN states are therefore necessarily also spin-triplet, and the characteristics of the reactions (1) thereby reflect the properties of the spin-triplet YN potentials alone. This simplifies the interpretation of data on reaction (2) and, further, it gives a means of making some empirical distinction between the spin-singlet and spin-triplet YN interactions, thus allowing a test of the spin-triplet YN interaction independent of the spin-singlet YN interaction. Otherwise, at present, the YN scattering and reaction data give us only the spin average $\frac{1}{4}\{3\sigma(S=1) + \sigma(S=0)\}$ of their cross sections. Some further information distinguishing between $V_{\rm YN}(S=1)$ and $V_{\rm YN}(S=0)$, especially sensitive to their S-wave components, is obtainable from the binding energies of states of the light hypernuclei, but these are not two-baryon systems, so that there are other uncertainties which act against drawing clear conclusions from them.

The characteristics of the $K^- \to \pi^-$ reactions (1) near 0° also depend on the amplitudes $T(\overline{K}N \to \pi Y)$ near 0°. We have based our calculations on the tabulation

* A related counter experiment has been carried out by D'Agostini *et al.* (1981) using the 0° reaction $\pi^- d \to K^+(n\Sigma^-)$ at 1400 MeV/c.

of partial-wave amplitudes, published first by Gopal *et al.* (1977) and then updated by G. P. Gopal (personal communication 1981), which were based on an energy-dependent analysis taking into account all of the $\bar{K}N$ two-body data available at the time. In order to avoid the rounding errors inherent in the use of the printed tables, a table of all the 0° $\bar{K}N \to \pi Y$ amplitudes was constructed versus momentum p_K, directly from the partial-wave analysis tapes (G. P. Gopal, personal communication 1981). The relationship between the isospin amplitudes, M_I for $\bar{K}N \to (\pi\Sigma)_I$ and N_1 for $\bar{K}N \to \Lambda\pi$, and the physical amplitudes is given in Table 1, together with the Gopal values and the observed cross sections. It is clear that an energy-independent partial-wave analysis, i.e. an analysis using the data at 700 MeV/c alone, can determine directly the magnitudes of M_0 and M_1, and their relative phase (again, in magnitude but not in sign), but the input data carries no information bearing on the phase of N_1 relative to those of M_0 and M_1. Consequently, in attempting to fit the 700 MeV/c data on reaction (2), we have multiplied the Gopal amplitude N_1 by a phase factor $\exp(-i\phi)$ and explored the variation of the predicted cross sections with ϕ, since the amplitudes $(M_0, M_1, N_1 \exp(-i\phi))$ necessarily give precisely the same fit to the input data at 700 MeV/c as do the amplitudes (M_0, M_1, N_1). This situation will be discussed further in Section 3.

Table 1. Amplitudes and cross sections used in the present work

The 700 MeV/c $\bar{K}N \to \pi Y$ amplitudes at 0° are expressed in terms of the isospin amplitudes M_0, M_1 and N_1. The values used in this work, by G. P. Gopal (personal communication 1981), but normalized such that $d\sigma(0°)/d\Omega = |\text{Amp}|^2$, are used to calculate the 0° differential cross sections, which are then compared with the input data (Armenteros *et al.* 1970)

Cross section	$K^-p \to$	Amplitude	Gopal (fm)	$(d\sigma/d\Omega)\|_{0°}$ (mb sr^{-1}) Gopal	Exp.
σ_+	$\Sigma^+\pi^-$	$-\sqrt{\frac{1}{6}}M_0 + \frac{1}{2}M_1$	$0{\cdot}0245 + 0{\cdot}048\,i$	0·029	$0{\cdot}09 \pm 0{\cdot}04$
σ_0	$\Sigma^0\pi^0$	$\sqrt{\frac{1}{6}}M_0$	$0{\cdot}1215 + 0{\cdot}0145\,i$	0·149	$0{\cdot}20 \pm 0{\cdot}04$
σ_-	$\Sigma^-\pi^+$	$-\sqrt{\frac{1}{6}}M_0 - \frac{1}{2}M_1$	$-0{\cdot}267 - 0{\cdot}080\,i$	0·777	$0{\cdot}50 \pm 0{\cdot}08$
σ_Λ	$\Lambda\pi^0$	$-\sqrt{\frac{1}{2}}N_1$	$0{\cdot}267 - 0{\cdot}0215\,i$	0·718	$0{\cdot}59 \pm 0{\cdot}10$

The fact that the ΣN threshold peak in reaction (2) is a cusp has been known for a long time, following the work of Karplus and Rodberg (1959) and Kotani and Ross (1959) on K^- capture from rest in deuterium. A few calculations have been reported for the in-flight reaction (2) in our momentum region by Satoh *et al.* (1975), Satoh (1976), Ryang and Saito (1976), Kimura *et al.* (1981) and Kimura (1982) for 400 MeV/c, and by Nishimura (1978) for 700 MeV/c, these calculations all being made on the basis of simple central separable potentials for the (ΛN, ΣN) systems, as well as by Dosch and Hepp (1978) for 700 MeV/c using dispersion-theoretic methods, and by Mizuno (1979) for 700 MeV/c using OBE potentials developed by himself. However, the physical situation at 400 MeV/c is somewhat special since this is the momentum at which the narrow resonance Λ(1520) is excited. Calculations using realistic YN potentials are very desirable, since there is now a good deal of knowledge about these potentials, and Hemming (1978) carried out the first such calculation, using the BDI-1 and BDI-2 potentials of Brown *et al.* (1970), with some success but with some unintentional omissions. In the present work, the aims are to improve the computational program, so that the F potential of Nagels *et al.* (1979)

can be tested, to rectify the omissions, and to extend the computations to include other reaction channels.

In Section 2 we shall set up the formalism, explain what has to be calculated and what physical input will be used, and lay out the calculational procedure. In Section 3 we shall discuss the results of these calculations, in relation with the data, choosing the optimum value for ϕ. An alternative procedure for carrying out such analyses in future will be discussed, which may be helpful for the planning of further experiments on these deuterium reactions.

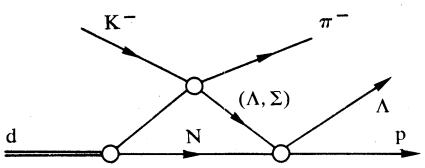

Fig. 2. Triangle graphs for the process $K^-d \to \Lambda p\pi^-$.

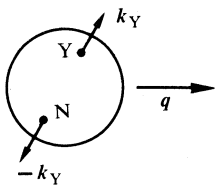

Fig. 3. Kinematics of the final YN system in the lab frame.

2. Kinematics and the Calculation of Reaction Amplitudes

With the neglect of multiple-scattering corrections, the essential reaction mechanism is as depicted in Fig. 2. The $K^- \to \pi^-$ transition transfers an energy ε and a momentum $\boldsymbol{q}$ to the two-baryon system, giving rise to the strangeness-changing transition $d \to YN$. Its kinematics are depicted in Fig. 3. By definition, the energy transfer ε is

$$\varepsilon = (m_K^2 + p_K^2)^{\frac{1}{2}} - \{m_\pi^2 + (\boldsymbol{p}_K - \boldsymbol{q})^2\}^{\frac{1}{2}}. \tag{5}$$

The total c.m. energy in the final YN system will be denoted by m_{YN}. Its relationship with the c.m. momentum $\boldsymbol{k}_Y$ for this system is given by

$$m_{YN} = (m_N^2 + k_Y^2)^{\frac{1}{2}} + (m_Y^2 + k_Y^2)^{\frac{1}{2}}. \tag{6}$$

In baryonic variables, the energy transfer may be written alternatively as

$$\varepsilon = (m_{YN}^2 + q^2)^{\frac{1}{2}} - m_d. \tag{7}$$

Our interest is in forward scattering ($\cos\theta_{K\pi} \geqslant 0{\cdot}9$) and the momentum transfer is then sufficiently small for nonrelativistic approximations to be made. For $\theta_{K\pi} = 0°$, a plot of q as function of p_K and m_{YN} has been given by Dalitz (1979), where it will be seen that, for $p_K = 700$ MeV/c, q varies from 37 MeV/c for the ΛN threshold, and 93 MeV/c for the ΣN threshold, to 120 MeV/c for $m_{YN} = 2160$ MeV. When $\theta_{K\pi} \neq 0°$, but $\cos\theta_{K\pi} \geqslant 0{\cdot}9$, $\boldsymbol{q}$ has also a component transverse to $\boldsymbol{p}_K$, with magnitude of order $p_K \sin\theta_{K\pi}$, which is less than about 200 MeV/c. With the nonrelativistic approximation the above relations (6) and (7) reduce to

$$m_{YN} \approx m_N + m_Y + k_Y^2/(2\mu_{YN}), \tag{8}$$

$$\varepsilon \approx m_N + m_Y - m_d + k_Y^2/(2\mu_{YN}) + q^2/2(m_Y + m_N), \tag{9}$$

where μ_{YN} denotes the YN reduced mass. The lab recoil momentum given to the nucleon is then given by

$$\boldsymbol{p}_{N_1} = \{m_N/(m_Y+m_N)\}\boldsymbol{q} - \boldsymbol{k}_Y, \tag{10}$$

and an empirical cut-off $p_N \geqslant p_{cut}$, such as holds for the data of Braun *et al.* (1977), corresponds to the constraint†

$$\cos\theta \leqslant [\{m_N/(m_Y+m_N)\}^2 q^2 + k_\Lambda^2 - p_{cut}^2](m_Y+m_N)/2m_N q k_Y, \tag{11}$$

where θ is the angle between $\boldsymbol{q}$ and $\boldsymbol{k}_Y$.

The reaction amplitude for $K^- d \to \Lambda p \pi^-$, corresponding to Fig. 2, has the general structure (Dalitz and Deloff 1982)

$$T(K^- d \to \Lambda p \pi^-) = \int \{-\sqrt{\tfrac{1}{2}}\, N_1\, \phi^*_{\Lambda\Lambda}(\boldsymbol{r}) + \text{ZERO}\, \phi^*_{\Lambda\Sigma^0}(\boldsymbol{r}) + \text{PLUS}\, \phi^*_{\Lambda\Sigma^+}(\boldsymbol{r})\}$$
$$\times \psi_d(\boldsymbol{r}) \exp(i\,\boldsymbol{Q}.\boldsymbol{r})\, d\boldsymbol{r}, \tag{12}$$

where $\boldsymbol{r}$ denotes the separation between the two baryons, $\boldsymbol{Q} = \boldsymbol{q} m_N/m_{YN}$, and the coefficients are

$$\text{PLUS} = -\sqrt{\tfrac{1}{6}}\, M_0 + \tfrac{1}{2} M_1, \qquad \text{ZERO} = -\sqrt{\tfrac{1}{2}}\, M_1. \tag{13a, b}$$

The wavefunctions $\phi_{ij}(\boldsymbol{r})$ are the components of the YN wavefunction for an outgoing plane wave in the channel i (here Λp) with ingoing spherical waves in all channels j. Thus, in our present case, the YN wavefunction is required to have the following asymptotic form:

$$\psi_\Lambda^{(-)}(\boldsymbol{r}) = \begin{pmatrix} \phi_{\Lambda\Lambda}(\boldsymbol{r}) \\ \phi_{\Lambda\Sigma^0}(\boldsymbol{r}) \\ \phi_{\Lambda\Sigma^+}(\boldsymbol{r}) \end{pmatrix} \xrightarrow[r\to\infty]{} \begin{pmatrix} \exp(i\boldsymbol{k}_\Lambda.\boldsymbol{r}) + T(\Lambda p \to \Lambda p)^* \exp(-i k_\Lambda r)/r \\ T(\Lambda p \to \Sigma^0 p)^* \exp(-i k_{\Sigma^0} r)/r \\ T(\Lambda p \to \Sigma^+ n)^* \exp(-i k_{\Sigma^+} r)/r \end{pmatrix}, \tag{14}$$

where $T(YN \to YN)$ denote the appropriate elements of the YN T matrix. For brevity, we have written out explicitly only the S-wave components for the deuteron and the YN wavefunctions, which correspond to $S \to S$ transitions in the amplitude (12). These are, of course, the essential components for the threshold phenomena we are concerned with. However, the deuteron wavefunction does have a substantial $^3D_1$ component, and the YN interactions generally include a strong tensor potential, which couples $^3D_1$ YN states with the $^3S_1$ YN states; the resulting contributions to (12) from the $NN \to YN$ transitions $^3S_1 \to {}^3D_1$, $^3D_1 \to {}^3S_1$ and $^3D_1 \to {}^3D_1$ have all been included in the calculations reported here. The spin variable has been suppressed in expression (12), but this gives correctly the dominant transition amplitude ($^3S_1 \to {}^3S_1$). The additional angular-momentum projection operators required for transitions involving $^3D_1$ states have been included in our calculation. The tensor component of the YN interactions makes it essential to include the coupled

† The relativistic form for this constraint is

$$\cos\theta \leqslant [\{(m_{YN}^2+q^2)(m_N^2+k_Y^2)\}^{\frac{1}{2}} - m_{YN}(m_N^2+p_{cut}^2)^{\frac{1}{2}}]/qk_Y.$$

($^3S_1$–$^3D_1$) partial waves, since the striking peak shown in Fig. 1 at mass $m_{YN} \approx m_\Sigma + m_N$ is associated with the ($\Lambda N, \Sigma N$) $^3S_1$ state. For simplicity, YN interactions have been neglected in all other partial waves, although they might well have substantial effects in other mass regions; for example, the ^3P YN interactions might well affect the m(YN) distribution appreciably in the valley between the ΛN and ΣN threshold peaks. The use of plane waves for all states other than ($^3S_1$–$^3D_1$) means that the amplitude (12) can be evaluated for non-forward angles without further numerical integrations—at least for angles $\theta_{K\pi}$ such that the $\bar{K}N \to \pi Y$ spin-flip amplitudes can be neglected in square—the total amplitude then being given by the impulse approximation amplitude with the ($^3S_1$–$^3D_1$) part projected out and replaced by the numerically calculated ($^3S_1$–$^3D_1$) amplitude, which does not depend on the angle between $\boldsymbol{q}$ and $\boldsymbol{k}_Y$ (Dalitz and Deloff 1982). In general, the $\theta_{K\pi}$ dependence of the non-spin-flip amplitudes M_0, M_1 and N_1 will also need to be taken into account.

The wavefunctions $\phi_{ij}(r)$ needed to evaluate (12) were calculated by integrating numerically the six-channel Schrödinger equations (Λp, $\Sigma^+ n$ and $\Sigma^0 p$, each for $^3S_1$ and $^3D_1$ waves) for the given YN potential, using the observed baryon masses in the kinetic energy terms, subject to the boundary conditions (14) at infinity. The results reported here are mostly for the NSR-F potential, the last and most elaborate of the one-boson-exchange (OBE) YN potentials developed by Nagels *et al.* (1979). The parameters of these potentials were chosen to fit all of the ΛN and ΣN cross sections known, which pertain mostly to the S waves near the ΛN and ΣN thresholds, with physical meson masses and with meson–baryon coupling parameters chosen to fit SU(3) constraints, or to correspond with known SU(3)-breaking patterns. For contrast, we also considered the earliest OBE YN potential proposed, the BDI-1 potential of Brown *et al.* (1970), fitted to the early ΛN and ΣN data but with a simpler meson-exchange structure, fewer mesons being known at that early time. The main contrast between these two potentials lies in their tensor character: the BDI-1 potential is dominated by σ exchange and has quite weak tensor components, whereas NRS-F has such strong tensor components that it predicts a broad $^3D_1$ resonance just below the ΣN threshold. Also, the BDI-1 potential predicts an unstable bound-state resonance in the ΛN $^3S_1$ wave, about 40 keV below the ΣN threshold in the charge independent limit (i.e. coincidence of $\Sigma^+ n$ and $\Sigma^0 p$ thresholds), whereas NRS-F does not predict any $^3S_1$ wave resonance.

With the amplitudes (12), the required cross section is proportional to

$$\sum |T(K^- d \to \Lambda p \pi^-)|^2 \delta[(m_K^2 + p_K^2)^{\frac{1}{2}} + m_d - (m_\pi^2 + p_\pi^2)^{\frac{1}{2}} - \{m_{YN}^2 + (\boldsymbol{p}_K - \boldsymbol{p}_\pi)^2\}^{\frac{1}{2}}] \times p_\pi^2 \, dp_\pi \, d\Omega_{K\pi} \, k_Y^2 \, dk_Y \, d\Omega_Y / (m_\pi^2 + p_\pi^2)^{\frac{1}{2}}, \quad (15)$$

apart from constant factors, the sum being taken over both initial and final spin states. The pion direction is given by $\theta_{K\pi}$ (lab frame); p_π is then determined by energy conservation, for definite m_{YN}. The momentum k_Y is fixed by m_{YN} and dk_Y is to be replaced by $(dk_Y/dm_{YN})dm_{YN}$, from relation (8). The only integration necessary is over the direction of $\boldsymbol{k}_Y$ relative to $\boldsymbol{q}$, and this can be carried out analytically when only the ($^3S_1$–$^3D_1$) YN interaction is included, whether or not $\boldsymbol{q}$ is parallel to $\boldsymbol{p}_K$. This θ integration is subject to the inequality (11), and it is well known that this is a strong constraint, in general. For K^+–deuterium reactions (Hendrickx *et al.* 1967), about two-thirds of the events have a recoil momentum less than 75 MeV/c. In

the present case, the constraint is especially strong for events with $\theta_{K\pi} = 0°$. The momentum transfer q is then about 37 MeV/c over the ΛN peak, so that the event rate will be zero until k_Λ reaches a value about 57 MeV/c, i.e. for $m_{YN} \leqslant 2057$ MeV. The reason the empirical data (Fig. 1) show a high rate for events in this mass region is that they integrate over a finite solid angle $d\Omega_{K\pi}$, thereby including the nonzero contributions from $\theta_{K\pi} \neq 0°$. Any calculated spectrum must therefore integrate over the full range of $\theta_{K\pi}$, here $\cos\theta_{K\pi} \geqslant 0{\cdot}9$, included in the experimental data with which it is to be compared. Fortunately, as noted above, the inclusion of angles $\theta_{K\pi} > 0°$ does not require us to integrate any further Schrödinger equations, but only adds a trivial numerical integration over $\theta_{K\pi}$, at least within the approximations accepted in this paper.

We note next that N_1 interferes with the terms ZERO and PLUS in (15), so that the phase of N_1 affects the final cross section. If we denote by χ the phase of N_1 relative to PLUS, the calculated cross section has the following dependence on χ:

$$d\sigma/dm_{YN} = A + B\cos\chi + C\sin\chi, \tag{16}$$

where B and C approach zero as $N_1 \to 0$. The tabulations available on M_0, M_1 and N_1, as functions of energy p_K and angle $\theta_{K\pi}$ (Gopal *et al.* 1977; G. P. Gopal personal communication 1981), do specify a definite phase for N_1, but we shall consider here the possibility of arbitrarily varying this phase to find the best fit to the 700 MeV/c data in Fig. 1. In a previous paper (Dalitz and Deloff 1982), we changed both the magnitude and phase of N_1 arbitrarily, simply to demonstrate that the empirical distribution, especially the prominence of the ΣN cusp relative to the ΛN threshold peak, could be fitted for *some* choice of the $\bar{K}N \to \pi Y$ amplitudes. However, that choice corresponded to increasing the $K^-p \to \Lambda\pi^0$ cross section at 700 MeV/c by a factor of 4, and that is quite definitely inadmissible.

3. Results and Discussion

The Gopal amplitudes summarized in Table 1 lead to the following values for the coefficients in the integral (12):

$$\text{PLUS} = 0{\cdot}0245 + 0{\cdot}048\,\text{i fm}, \tag{17a}$$

$$\text{ZERO} = -0{\cdot}206 - 0{\cdot}0905\,\text{i fm}, \tag{17b}$$

$$\sqrt{\tfrac{1}{2}}N_1 = -0{\cdot}267 + 0{\cdot}0215\,\text{i fm}. \tag{17c}$$

The phase of N_1/PLUS is 67·6°. We change this phase to

$$\chi = (67{\cdot}6 - \phi)°. \tag{18}$$

We note first that the ΛN peak varies very little with ϕ, because the intermediate ΣN wave is damped like $\exp(-\kappa r)$, where $\kappa \approx \{2\mu_{\Sigma N}(m_\Sigma - m_\Lambda)\}^{\frac{1}{2}} \approx 1{\cdot}44\,\text{fm}^{-1}$ in this region. Its amplitude at the other nucleon is roughly measured by $\exp(-\kappa R) \approx 1/500$, where R denotes the deuteron radius $1/(m_N B_d)^{\frac{1}{2}}$. Thus, the amplitudes PLUS and ZERO have little effect on the ΛN peak; only N_1 contributes significantly and its phase is then irrelevant for the cross section $d\sigma/dm_{YN}$ in this region.

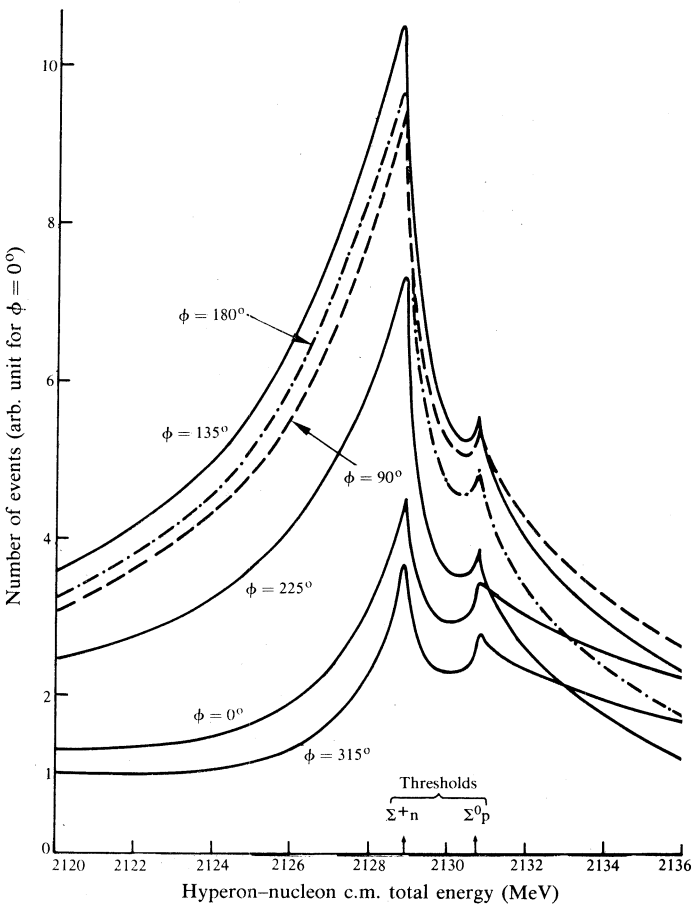

Fig. 4. The $m_{\Lambda p}$ mass distribution in the ΣN threshold region, calculated for the NRS-F YN potential and the 700 MeV/c Gopal amplitudes (with added phase ϕ to the amplitude N_1), as a function of this phase ϕ. (The curves for $\phi = 90°$ and 180° are shown as dashed and dot–dash lines respectively, only in order to make them distinguishable from the $\phi = 135°$ curve.)

The distributions $d\sigma/dm_{YN}$ in the region of the ΣN threshold are shown for the NRS-F potential for various values of the angle ϕ in Fig. 4. We note that:

(i) the peak at the Σ^+n threshold is higher than that at the Σ^0p threshold, for all ϕ;

(ii) the sharpness of each peak varies with ϕ (see below);

(iii) the effect of the interference due to N_1 is complicated, but an increase from $\phi = 0°$ raises both Σ^+n and Σ^0p peaks, the effect being maximal for $\phi = 140°$, and of course symmetrical for ϕ on either side of this value. The same is true on the lower side of the Σ^+n peak; for example, the intensity at 2125 MeV is also maximal at $\phi = 140°$. On the upper side of the peak, the intensity is maximal for ϕ closer to 90°; for example, at 2133·5 MeV, the phase angle for maximal intensity is 95°. Hence the best fit for the shape of the m_{YN} distribution over the ΣN threshold region would be somewhere between $\phi = 95°$ and 135°. Indeed, any value for ϕ in this range would provide an acceptable fit to the data.

For calculations with BDI-1 potentials, essentially the same remarks hold, except that at 2133·5 MeV, the symmetry axis for the ϕ distribution is at 102°, a little larger angle than for NRS-F. Our general conclusion is that any value of ϕ between 105° and 135° would give an acceptable fit, for either potential. We have not attempted to find the best overall value for ϕ, for reasons mentioned below.

For the purpose of illustration, here and below, we have chosen $\phi = 135°$. The resulting m_{YN} distribution for NRS-F, with $p_{cut} = 75$ MeV/c, is plotted in Fig 1 and compared in shape with the data over the full range of m_{YN}; the ordinate scale has been adjusted freely to give the best fit by eye. The intensity of the ΛN peak (all $m_{YN} \leqslant 2070$ MeV) relative to the ΣN peak ($m_{YN} = 2130 \pm 10$ MeV) is about right, but the ΣN peak calculated appears tilted relative to the data, predicting too many events in the range 2120–9 MeV below Σ^+n threshold and too few events in the range 2129–40 MeV above this threshold. The remarks in the last paragraph indicate that a better fit to the shape in the ΣN peak region would be obtained if ϕ were brought down to 105° (say), but the total number of events predicted for the ΣN peak would thereby be reduced. It must also be pointed out that the number of events in the ΛN peak is quite sensitive to the p_{cut} adopted and, further, that the constraint applied by Braun *et al.* (1977) is probably* $|\boldsymbol{p}_{\|}| \geqslant p_{cut}$, where $\boldsymbol{p}_{\|}$ is the component of the proton recoil momentum in the plane perpendicular to the mean of the camera directions, rather than $|\boldsymbol{p}| \geqslant p_{cut}$, as we have adopted in these calculations. The data also show an excess of events in the range 2075–95 MeV, but this is the region of m_{YN} where the ^{3}P YN interactions which we have neglected could be most effective.

For $\phi = 135°$, the m_{YN} distribution for $p_{cut} = 150$ MeV/c is quite compatible with the data (shaded area in Fig. 1). The ΣN peak is little affected by the cut, since the at-rest reaction ΣN → ΛN gives a c.m. momentum 280 MeV/c to the nucleon. The cut has a strong effect on the distribution below 2100 MeV but the prediction agrees tolerably well with the data. There is no uncertainty about the interpretation of this cut, since the recoil protons have quite long tracks and are clearly visible, even if perpendicular to the mean focal plane for the cameras.

The detail of the ΣN threshold peaks is shown for $\phi = 135°$ in Fig. 5 by plotting the cross sections against (*a*) the c.m. momentum k_{Σ^+} for the lower peak, and (*b*) the c.m. momentum k_{Σ^0} for the upper peak. The Σ^+n threshold plot in (*a*) shows that its cusp is S-shaped, the slope $d\sigma(\Lambda)/dk_{\Sigma^+}$ having the same sign (but different value) below and above the threshold. At the Σ^0p threshold in (*b*), the slope $d\sigma(\Lambda)/dk_{\Sigma^0}$ is positive below, and negative above, the threshold, so the cusp there (although small) is predicted to be upward. Plots of $\sigma(\Lambda)$ are also given in Fig. 5 for other values of ϕ in order to show that the form of the cusp does depend appreciably on the interference phase angle ϕ. The Σ^+n threshold cusp in $\sigma(\Lambda)$ is upward for $\phi = 0°$, whereas it is S-shaped for $\phi = 135°$; for the intermediate case $\phi = 90°$, there is almost no cusp at all on the lower side of the threshold, and the same remark holds for $\phi = 180°$.

The total cross section $\sigma(\Lambda + \text{all } \Sigma)$ for the $K^- \to \pi^-$ transition on deuterium is plotted against m_{YN} in Fig. 1 (dashed curve), and against k_{Σ^+} and k_{Σ^0} in Fig. 5. For $\phi = 135°$, the slope $d\sigma(\Lambda + \text{all } \Sigma)/dk_{\Sigma^+}$ is negative below, and negative above, the Σ^+n threshold, giving a small S-shaped cusp; at the Σ^0p threshold, $d\sigma(\Lambda + \text{all } \Sigma)/dk_{\Sigma^0}$

* This point is not clear in the paper of Braun *et al.* Their remark on this point (see the second paragraph in Section 2) *does* specify the projected track length but in the same sentence they specify the cut-off as $|\boldsymbol{p}| \geqslant 75$ MeV/c.

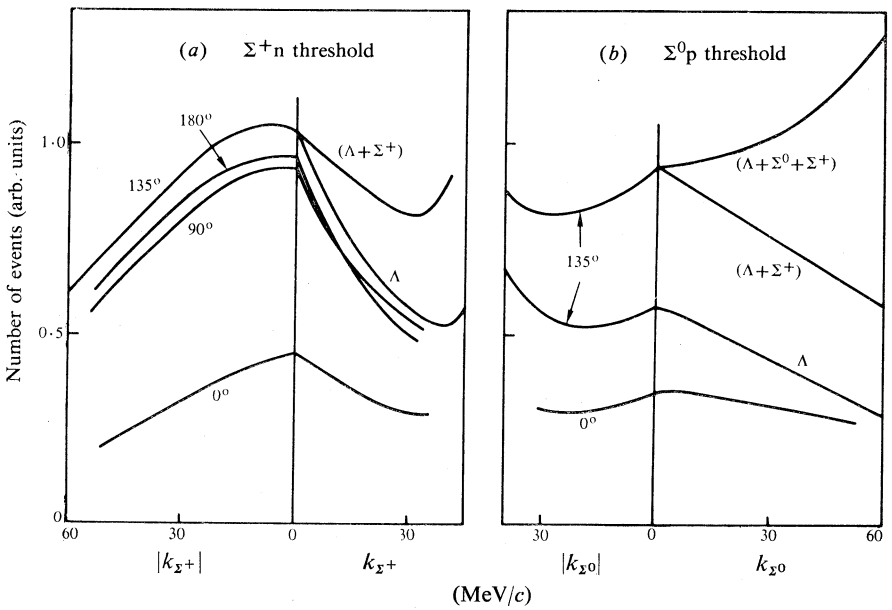

Fig. 5. Reaction cross sections are plotted against (*a*) the c.m. momentum k_{Σ^+} around the Σ^+n threshold and (*b*) the c.m. momentum k_{Σ^0} around the Σ^0p threshold, in order to show the detailed nature of the cusps occurring at these thresholds, for the case $\phi = 135°$ shown in Fig. 6. The other plots are for the $\Lambda p\pi^-$ cross section alone to illustrate that the character of the cusp does vary with the value of ϕ. These curves are all calculated with the NRS-F potential.

is positive both below and above, so this cusp is also S-shaped. An S-shaped cusp is generally difficult to see, and the dashed curve in Fig. 1 is no exception to this statement. The total cross section shows a small bump at the Σ^+n threshold, which could certainly not be seen with the present experimental resolution. This total cross section can be determined by direct measurement of the $K^- \to \pi^-$ transition rate on a deuterium target, without observation of the final hyperons; there exists only one such measurement in the literature, made at 800 MeV/*c* (May *et al.* 1982), but we consider it premature to attempt a comparison of it with our present calculations, since those data show some inconsistency with deuterium bubble chamber data.

We turn now to the comparison of the BDI-1 predictions for the $m_{\Lambda p}$ distribution with those for NRS-F. These two potentials are indistinguishable in the ΛN peak region. This is not surprising since they involve many of the same meson exchanges and have been fitted to the same low-energy Λp scattering data. They differ a little in their predictions for the ΣN peaks, shown in Fig. 6. They predict about the same total intensity over the range 2129 ± 6 MeV, but the BDI-1 curve appears tilted relative to the NRS-F, being lower than NRS-F below the Σ^+n threshold and higher above, in slightly better agreement with the data. With $\phi = 135°$, both potentials predict an S-shaped cusp at the Σ^+n threshold; with $\phi = 0°$, NRS-F predicts an upward cusp there, whereas BDI-1 predicts an S-shaped cusp. These are minor differences in relation to the accuracy and resolution with which these distributions can be measured experimentally at present, and we have to conclude that this experiment cannot yet hope to decide between these two potentials, despite their appreciably different spin structures. This is perhaps not surprising in view of the fact that both

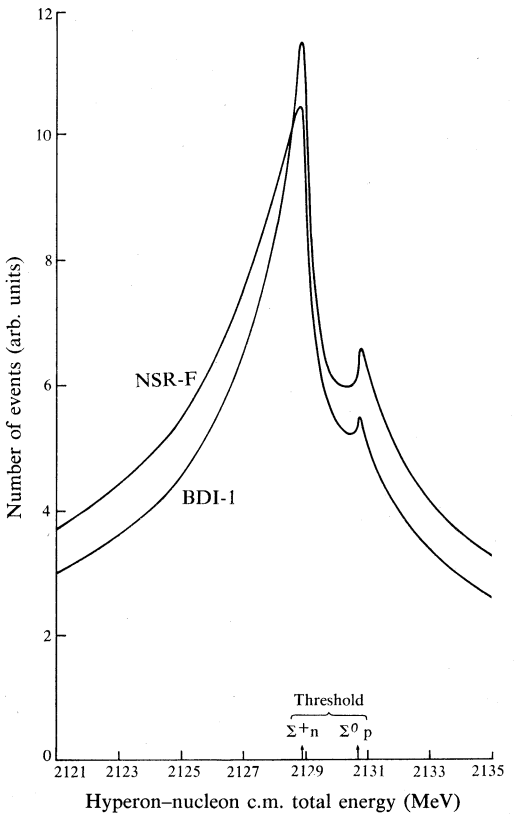

Fig. 6. Calculated m_{Ap} mass distributions in the ΣN threshold region are compared for the NRS-F and BDI-1 YN potentials, for the 700 MeV/c Gopal amplitudes with added phase $\phi = 135°$.

potentials have been arranged to fit much of the same scattering and reaction data in the ΛN and ΣN threshold regions.

Finally, it is of interest to discuss briefly the relation of the input amplitudes $T(\overline{K}N \to \pi Y)$ used here with the raw data on $\overline{K}N \to \overline{K}N$ and $\overline{K}N \to \pi Y$ differential and polarization angular distributions. The amplitudes tabulated by Gopal were obtained by making an energy-dependent partial-wave fit to all of these data over a specified total c.m. energy range, using some definite energy-dependent form for each partial-wave amplitude as a function of c.m. energy E, each containing a series of parameters determined by optimizing the fit to this large body of data. In the present work, we are concerned only with $E = 1652{\cdot}7$ MeV, corresponding to $p_K = 700$ MeV/c, and the corresponding Gopal $\overline{K}N \to \pi Y$ amplitudes which we have used above are given in Table 1. The 0° differential cross sections calculated from them are also given, and are compared with the data of Armenteros *et al.* (1970) to which they were fitted. The agreement is rather poor, although the cross sections for this particular momentum (699 ± 10 MeV/c lab momentum) and angle ($\cos\theta = 0{\cdot}95$) are clearly based on quite limited statistics. It must be emphasized that this energy-dependent fit is based on about 10^4 input data, so that a poor fit to one particular momentum and angle would contribute relatively little to the overall goodness of fit to the total data.

As a result, it would be more satisfactory to use $\overline{K}N$ data from an experiment covering just the momenta and angles relevant to the K^-d observations, so that the

elementary parameters needed for the calculation of the K^-d reactions are accurately known. For the $\bar{K}N \to \pi\Sigma$ reactions, a knowledge of the cross sections specified in Table 1 would allow us to conclude that

$$|\,\text{PLUS}\,| = \sigma_+^{\frac{1}{2}}, \qquad |\,\text{ZERO}\,| = (\sigma_+ + \sigma_- - 2\sigma_0)^{\frac{1}{2}}, \tag{19a, b}$$

$$\text{Re}(\text{PLUS}^*\,\text{ZERO}) = |\,\text{PLUS}\,|\,|\,\text{ZERO}\,|\cos\alpha_{PZ} = (4\sigma_0 - 3\sigma_+ - \sigma_-)/2\sqrt{2}, \tag{19c}$$

where α_{PZ} is the phase difference $\alpha_P - \alpha_Z$ between PLUS and ZERO. Clearly, this does not determine the sign of α_{PZ}. For the $K^-p \to \Lambda\pi^0$ reaction, the corresponding equation is

$$N_{1\frac{1}{2}}^{\frac{1}{2}} = -(2\sigma_\Lambda)^{\frac{1}{2}}\exp(i\,\nu), \tag{20}$$

where the phase ν is undetermined. If we assume that the YN interaction is known, the new information provided by the K^-d reaction data is the phase ν relative to (say) the phase of PLUS, at least within two possibilities, one for each sign of α_{PZ}.

The present $\bar{K}N \to \pi Y$ data at 700 MeV/c do not yet allow a useful determination of ν. The quantity $\sigma_+ + \sigma_- - 2\sigma_0$ has the value $0{\cdot}19 \pm 0{\cdot}12$ mb sr^{-1}, while $4\sigma_0 - 3\sigma_+ - \sigma_-$ is $+0{\cdot}03 \pm 0{\cdot}24$ mb sr^{-1}. These lead to $|\,\text{PLUS}\,| = 0{\cdot}32 \pm 0{\cdot}07$, $|\,\text{ZERO}\,| = 0{\cdot}14^{+0.04}_{-0.06}$, and $\cos\alpha_{PZ} = +0{\cdot}1 \pm 0{\cdot}8$, so that α_{PZ} at 700 MeV/c is essentially undetermined by the empirical data at this momentum. Improvement of this $\bar{K}N \to \pi Y$ input data will be an essential element in a full understanding of the K^-d reaction data.

4. Conclusions

We have reported calculations of the m_{YN} distribution in the reaction $K^-d \to \Lambda p\pi^-$ for a K^- lab momentum of 700 MeV/c for two possible YN potentials, BDI-1 and NRS-F, which show that data with the resolution and statistics available at present are not sufficient to discriminate between them, despite the very considerable difference between their detailed structure. This may reflect the fact that the two potentials have each been adjusted to fit similar data on ΛN and ΣN scattering at low c.m. kinetic energy, but the degree of agreement may also be somewhat fortuitous.

The predictions show greater sensitivity to the $\bar{K}N \to \pi Y$ amplitudes used as input. At 700 MeV/c the $\pi\Lambda$ amplitude is by far the largest but its contribution to the ΛN threshold region is greatly reduced by the empirical cut made to exclude final states where the proton recoil momentum is small. It is pointed out above that the input amplitudes needed are not fully specified by data on all the $K^-p \to \pi Y$ reactions at one energy, whereas the relative phase between the $\pi\Lambda$ amplitude and the $\pi\Sigma$ amplitudes appears to be already determined, according to the published tables of 0° amplitudes resulting from partial-wave analyses (G. P. Gopal, personal communication 1981). The phase which appears to be determined in this way is partly an artifact of the energy-dependent partial-wave analysis procedure adopted, in that the result may depend on the analytic form chosen to represent the amplitude as a function of energy over the finite energy range covered in the analysis. The only other phase information which is input into the energy-dependent analysis is the fact that the amplitudes must have definite relative signs at those mass values corresponding to Σ^* and Λ^* resonances of known SU(3) character. For the relative phase of interest to us here, only the Σ^* states carry such information, and these states are few in number within the mass range covered by the partial-wave analyses

in question; hence we are led to question the definiteness with which the $(\bar{K}N \to \pi\Lambda)/(\bar{K}N \to (\Sigma N)_I)$ phase has been so determined. Since the amplitudes from intermediate $\pi\Lambda N$ and $\pi\Sigma N$ states in the strangeness-exchange process interfere, we have used this interference to determine the optimum value for the phase χ to be assigned to the $\pi\Lambda$ 0° amplitude relative to the $\pi\Sigma$ 0° amplitudes. Although this interference has a strong effect on the ΣN threshold region, it does not allow a precise determination of χ; values of χ over an arc of about 45° are all quite acceptable. It appears that it would be desirable to include data on the $K^- d \to \Lambda p \pi^-$ reaction as part of the input for a $\bar{K}N \to \pi Y$ partial-wave analysis.

Acknowledgments

We would like to thank Mr M. Torres for some help with running the computer programs necessary. This paper is dedicated to the memory of Stuart Butler, at one time a fellow student of one of us (R.H.D.) in Professor R. E. Peierls's Department of Mathematical Physics in the University of Birmingham. Professor Butler would have had interesting comments to make on this paper and is now much missed.

References

Alexander, G., Hall, B., Jew, N., Kalmus, G., and Kernan, A. (1969). *Phys. Rev. Lett.* **22**, 483.
Armenteros, R., *et al.* (1970). *Nucl. Phys.* B **21**, 15.
Bonazzola, G. C., *et al.* (1970). Search for production of hypernuclei by K^- interactions in flight—a missing-mass experiment. Internal Document CERN PH III-70/5.
Braun, O., *et al.* (1977). *Nucl. Phys.* B **124**, 45.
Brown, J. T., Downs, B. W., and Iddings, C. K. (1970). *Ann. Phys. (New York)* **60**, 148.
Cline, D., Laumann, R., and Mapp, J. (1968). *Phys. Rev. Lett.* **20**, 1452.
D'Agostini, G., *et al.* (1981). *Phys. Lett.* B **104**, 330.
Dalitz, R. H. (1979). *In* 'Meson–Nucleon Physics—1979 (Houston)' (Ed. E. V. Hungerford), p. 621 (American Inst. Phys.: New York).
Dalitz, R. H., and Deloff, A. (1982). *Czech. J. Phys.* B **32**, 1021.
Dosch, H. G., and Hepp, V. (1978). *Phys. Rev.* D **18**, 4071.
Eastwood, D., *et al.* (1971). *Phys. Rev.* D **3**, 2603.
Feshbach, H., and Kerman, A. K. (1966). *In* 'Preludes in Theoretical Physics' (Eds A. De-Shalit *et al.*), p. 260 (North-Holland: Amsterdam).
Glauber, R. E. (1959). *In* 'Lectures in Theoretical Physics' (Eds W. E. Brittin and L. G. Dunham), Vol. 1, p. 315 (Interscience: New York).
Gopal, G. P., *et al.* (1977). *Nucl. Phys.* B **119**, 362.
Hemming, C. R. (1978). D.Phil. Dissertation, Oxford University.
Hendrickx, K., *et al.* (1967). *Nucl. Phys.* B **112**, 189.
Karplus, R., and Rodberg, L. (1959). *Phys. Rev.* **115**, 1058.
Kerman, A. K., and Lipkin, H. J. (1971). *Ann. Phys. (New York)* **66**, 738.
Kimura, M. (1982). Ph.D. Dissertation, Science University of Tokyo.
Kimura, M., Iwamura, Y., and Takahashi, Y. (1981). *Prog. Theor. Phys. Jpn* **65**, 649.
Kotani, T., and Ross, M. (1959). *Nuovo Cimento* **14**, 1282.
May, M., *et al.* (1982). *Phys. Rev.* C **25**, 1079.
Mizuno, T. (1979). *Prog. Theor. Phys. Jpn* **62**, 1691.
Nagels, M. M., Rijken, T. A., and de Swart, J. J. (1979). *Phys. Rev.* D **20**, 1633.
Nishimura, A. (1978). An analysis of the Λp enhancement. Univ. Tokyo Preprint No. UT-309.
Povh, B. (1978). *Ann. Rev. Nucl. Part. Sci.* **28**, 1.
Ryang, S., and Saito, T. (1976). *Prog. Theor. Phys. Jpn* **56**, 1826.
Satoh, E. (1976). *Nucl. Phys.* B **102**, 51.

Satoh, E., Iwamura, Y., and Takahashi, Y. (1975). *Phys. Rev. Lett.* **35**, 1128.
Sims, W. H., O'Neall, J. S., Albright, J. R., Brucker, E. B., and Lannutti, J. E. (1971). *Phys. Rev.* D **3**, 2698.
Toker, G., Gal, A., and Eisenberg, J. M. (1981). *Nucl. Phys.* A **362**, 405.

Manuscript received 25 July, accepted 17 August 1983